

Shape Terra: mechanical feature recognition based on a persistent heat signature

Ramy Harik ^a, Yang Shi ^a and Stephen Baek ^{b,c}

^aUniversity of South Carolina, USA; ^bSeoul National University, Korea; ^cUniversity of Iowa, USA

ABSTRACT

This paper presents a novel approach to recognizing mechanical features through a multiscale persistent heat signature similarity identification technique. First, heat signature is computed using a modified Laplacian in the application of the heat kernel. Regularly, matrices tend to include an indicator to the manifold curvature (the cotangent in our case), but we add a mesh uniformity factor to overcome mesh proportionality and skewness. Second, once heat retention values are computed, we apply persistent homology to extract significant subsets of the global mesh at different time intervals. Subsets are computed based on similarity of heat retention levels and/or retention values. Third, we present a multiscale persistence identification approach where we scan the part at different persistence levels to detect the presence of a feature. Once features are recognized and their geometrical descriptors identified, the next stage in future work will be feature matching.

KEYWORDS

Shape matching; persistence; heat kernel; feature recognition

1. Introduction

Numerous ubiquitous benefits can be reaped of full or partial shape detection. Identification of similar mechanical parts (or sub-parts) can minimize cost for several trades: Design, Process Planning, Manufacturing, Prototyping, etc. The analyst can use previously generated process plans and manufacturing programs from existing parts to rapidly estimate the manufacturing cost of the new part. [16] details the diverse fields of application and forwards a qualitative overview of techniques. The latter are classified into (a) global feature-based; (b) manufacturing feature recognition-based; (c) graph-based; (d) histogram based; (e) product information-based; and (f) 3D object recognition-based. Recent research in shape recognition for multimedia parts matching is well advancing, investigating the novel concept of heat diffusion through the manifold [9]. However, results are not applicable as is to mechanical parts because they do not hold acute points, and if they exist (corners), they do not hold any meaning. In this study, we will first go into this recent breakthrough to recognizing primary design features. We will be mainly treating protrusions and pockets.

1.1. Parts taxonomy

It is imperative to clearly define part taxonomy to understand the type of parts we are attempting to recognize. We split parts into two main categories:

- Multimedia parts: These are not necessarily functional and are usually manufactured using plastic processes rather than material removal ones. Multimedia parts might constitute the complete product at hand and are not part of a bigger assembly. Typical examples are kids' toys such as the horse represented in Figure 1(a).
- Mechanical parts: These parts are typically functional components of a product and usually manufactured using traditional machining techniques. They usually have strength constraints which are obtained through a series of testing for endurance, failure and life cycles. Typical examples are the piston head, a connecting rod or a multi protrusion part such as the one represented in Figure 1(b).

1.2. Features attributes

Features represent the design intent of how a part was conceived, i.e.: when a profile is revolved around an axis we obtain a revolution feature. CAD software can list over 20 features obtained mainly through constructive solid geometry or through Boolean operations on 3D solids. The algorithm we are proposing will recognize features through an elimination process where the “leftovers” of a part do not hold any underlying representation. Features can be: protrusions, revolutions, pockets, thin features, base features, dimples, ribs, fillets, chambers, etc. At first, our work will handle protrusions and pockets.

CONTACT Ramy Harik  harik@cec.sc.edu

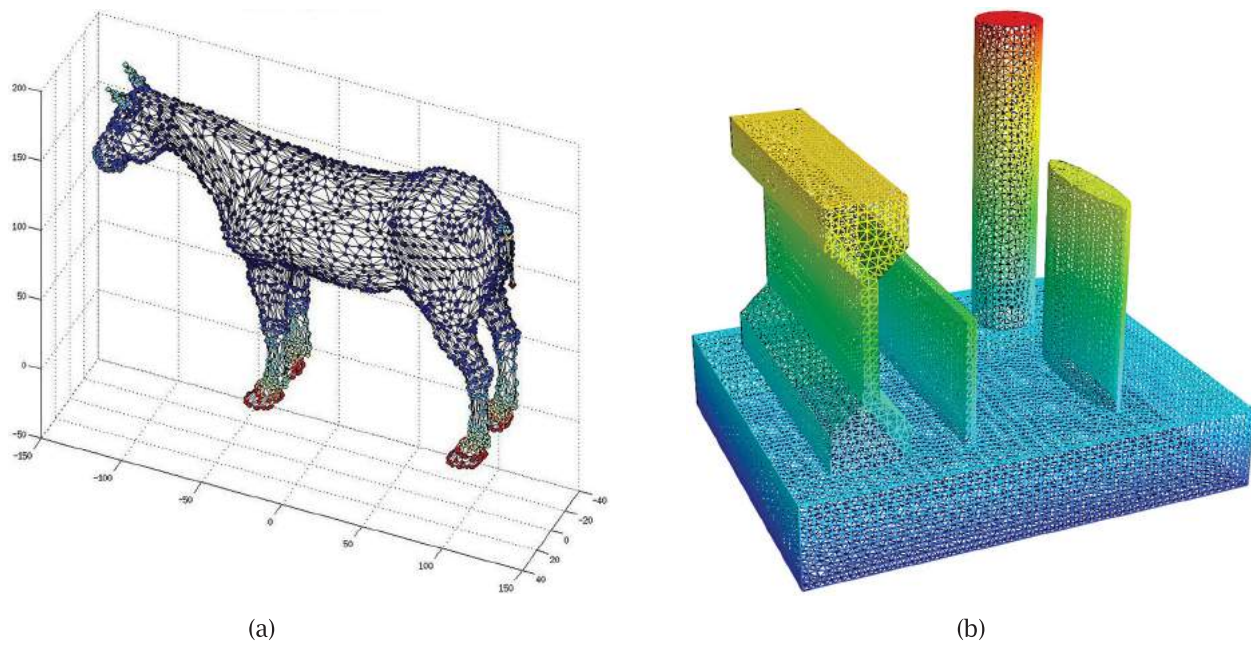


Figure 1. (a) Sample of a multimedia part. (b) Sample of mechanical part.

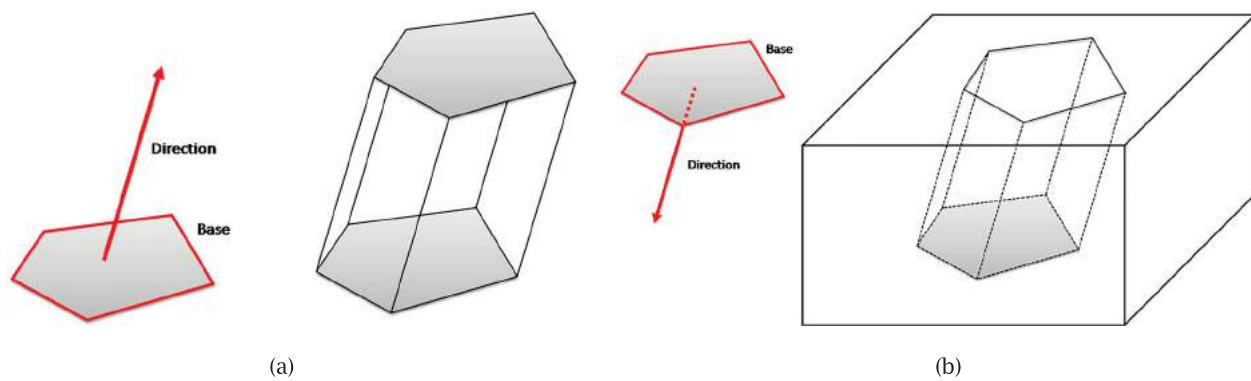


Figure 2. (a) Construction of a protrusion feature. (b) Construction of pocket feature.

Protrusions consist of a base extruded along a direction Figure 2(a). The base includes the profile or the cross section that will be elongated. The direction sets the orientation. Another major protrusion attribute is the protrusion height. Similarly, pockets are constructed through subtracting an extruded profile from a solid Figure 2(b). While their construction techniques and HKS might be deemed similar, a minor difference might arise relevant for feature recognition: the angles between cross section and faces are opposite. Software that will detect protrusions and pockets should detect three attributes of those features: cross section(s), direction, and height (or depth).

1.3. Goal and approach

The broader goal of this initiative is to generate a neutral methodology of feature classification. Ideally, the

user should be able to select a collection of points and run its analysis. The methodology should return features that exhibits similar heat retention properties as well as to identify the underlying mechanical properties and dimensions.

In the following sections, we will first present an extensive overview of the current state of the art. This section surveys literature on the heat kernel signature, persistent homology and shape descriptors. These three tools are used next to develop our algorithm. Our study analyzes heat values and heat retention levels at different clusters of a part to identify and categorize potential mechanical features. The overall methodology is presented next in Section 3. Here, the mathematical background behind the heat kernel and persistent homology is detailed in as well as the multiscale persistence clustering technique leading to feature recognition. Persistent homology is critical to properly identify connected subsets potentially

forming a feature. Section 4 presents the current development efforts, the parts database generated to test our algorithm and the current results. The article ends with future perspectives on further recognizing prominent features [13].

2. State of the art

In this section we survey the pertinent literature to conduct our shape identification technique. Previous feature recognition techniques were based on geometrical identification of feature components followed by an inter-connecting stage [3]. Some approaches were holistic looking at the macro-level identification of features, while others constructed elementary features at first, to be connected second [13]. The traditional literature classifies feature recognition techniques into variant, generative and neural network approaches [13,14]. These techniques dating from early process planning recognition efforts were trade oriented. Features were classified depending on the potential usage (form feature, manufacturing feature Figure 3 . . .). Our study overlooks traditional means of shape recognition and attempts to analyze heat values at different parts' clusters to identify and categorize potential mechanical features.

2.1. Shape signature and descriptors

The signature of a shape is a concise representation of the shape that captures some of its essence. It cannot be used to reconstruct the shape from it, nor fully represent the shape [12]. However it could be used in various applications if the signature succeeds in properly expressing some of the shape's properties. A typical

application is 3D shape similarity. In this application, signatures are determined from geometric objects and used to determine similarity. Instead of comparing the whole object, solely the signatures are compared thus accelerating the matching technique.

[12] introduces a new signature which is pose-oblivious in addition to being scale, translation, and rotation invariant. The signature is a 2D histogram which is a combination of the distribution of two scalar functions defined on the boundary surface of the 3D shape. One of the defined functions is a novel function introduced by the authors called the local-diameter function. Using this histogram alone causes the function to lose its spatial distribution. In order to compensate the former loss, a second measure is used, the centrality function which has the role of measuring for each point on the boundary surface of the object, the average of the geodesic distances to all other points on the mesh. However these geodesic distances are sensitive to local topological changes leaving representations that rely on them with limited robustness [19].

To avoid using the geodesic distances, the authors present the GPS embedding which is an invariant deformation representation of surfaces that is based on combining the Laplace-Beltrami eigenvalues and eigenfunctions. They introduce an invariant shape descriptor, a G2 distribution, which for a given surface computes the GPS embedding and then finds the D2 shape distribution of the GPS embedding. [17] presents a technique to render a descriptor invariant to bending hence enhancing its performance over databases that contain articulated shapes. The results of the benchmark showed that, overall, the heat kernel-based feature detectors perform best and heat kernel signatures show the best results among the compared ones. Heat kernel-based methods

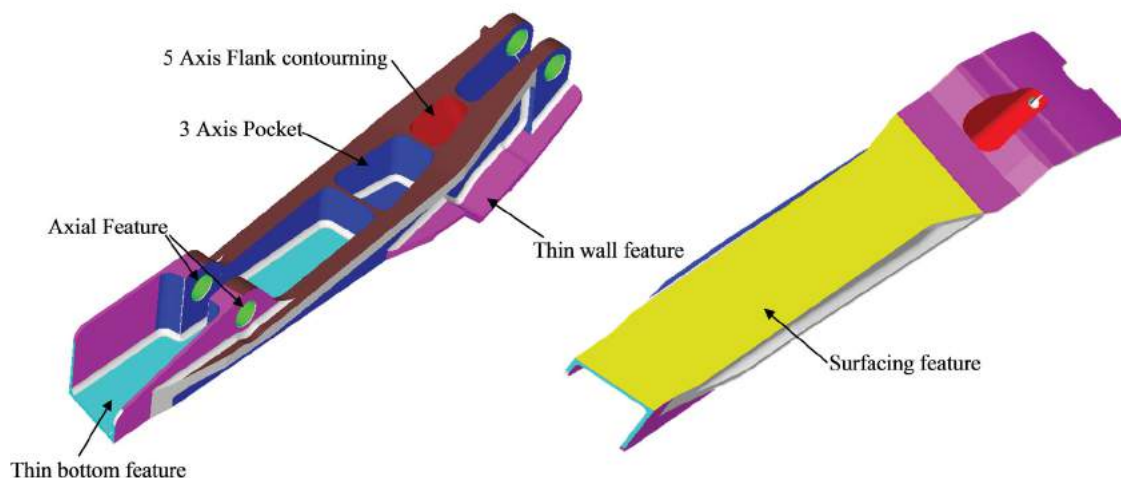


Figure 3. Previous results on manufacturing feature recognition, coded in CAA/CATIA © [13].

show high repeatability and perform best under many transformations, however for topological changes and holes 3D Harris detectors show best results [4].

One of the biggest challenges in the shape retrieval process is to have a descriptor that is invariant to as many transformations an object can experience. Moving on to descriptors that rely on the heat kernel, much research was done to render the heat kernel a multi scale descriptor. [9] says that the use of HKS at different time values allows the description of features at multiple scales. In order to identify local features, the HKS is applied on a short time period and for identifying global features, the signature is used on a larger time period. [11] develops a new shape descriptor called temperature distribution (TD) descriptor. Results showed the effectiveness of the TD descriptor within applications of 3D matching and searching for models at different poses and various noise levels. [5] develops an approach that does not use the time domain to make the heat kernel signature a multi scale descriptor. Shape recognition performed through heat is achieved by solving the heat equation over the geometry. [21] shows that the solution of the heat equation called the heat kernel is related to the eigenvalues and eigenfunctions of the Laplacian. The use of the Laplace operator along with the heat kernel is used to discover geometrical information about the manifolds. The link between the analysis of the geometry and the geometry itself is the eigenvalues of the Laplace operator. [2] develops an algorithm that approximates the Laplace operator on a meshed surface with point-wise convergence. The algorithm was empirically proved to exhibit convergence and outperforms other methods in accuracy and robustness with respect to noise data. [20] proposes a novel point signature that has the following desirable properties: it organizes information of a shape in an efficient and multi-scale way which is achieved by controlling the time of diffusion, it is stable under perturbations of the shape, it is concise but still informative, and it can be estimated faithfully and efficiently. The HKS inherits properties of being intrinsic and stable against perturbations of the shape from the heat kernel. [9] shows that the synergy between HKS and persistent homology leads to an efficient pose-oblivious matching algorithm that can be used for all models, whether partial, incomplete, or complete. Experimental results show that this method is effective in shape matching.

2.2. HKS centered shape recognition and persistence homology

The description of shape features with multidimensional nature must be done by a multidimensional measuring tool [6]. Generalization of persistent homology

modules can be achieved by the construction of size functions related to multidimensional measuring functions. [23] shows that the persistent homology of a filtered d -dimensional simplicial complex is simply the standard homology of a particular graded module over a polynomial ring. Their analysis establishes the existence of a simple description of persistent homology groups over arbitrary fields. It enables as well the derivation of a natural algorithm for computing topological spaces in an arbitrary dimension over any field. In order to improve the computation of persistent homology, [15] uses mesh generation to reduce the time and space complexity of computing the persistent homology of a point set. [22] presents fast algorithms that construct the filtered Vietoris-Rips complex of a point set. This complex is popular in topological data since it extends easily to higher dimensions. [7] develops the theory of zigzag persistent homology. This makes the advantages of persistent homology available but in a much greater generality. [8] develops a method for measuring homology classes. The authors provide an algorithm to compute the optimal basis and measure classes in it. [10] uses scale as a solution to assess the persistence of topological attributes and to prioritize simplification steps.

3. General approach

The following paragraph describes the approach adopted to recognize protrusions and pockets features. It follows the digital detection logic of Shape Terra, an application developed in Python. Input of Shape Terra is a triangular mesh with coordinates and vertices listed in a CATIA © mesh “.dat” file. Ideally, the software can be connected to other attempts at treating cloud of points obtained from a 3D scanning device and have its noise filtered and triangulation performed. Figure 4 shows the two traditional input methods leading to delivering a triangulated mesh. The latter is the input of Shape Terra. Different mesh sizes were tried (10 mm, 5 mm, 1 mm . . .) as well as non-uniform and uniform meshing. Refining our mesh would certainly lead to more accurate results, however at the expense of computation time. 2 mm uniform meshes gave good results while not being too computationally expensive.

3.1. Stage 1: heat retention signature

Throughout this stage, we attempt to estimate the heat losses a source endures through time. The rate, at which a source diffuses heat, is deemed an indicator on the localization of a point with respect to its surroundings. In order to do so, we attempt to solve the partial differential

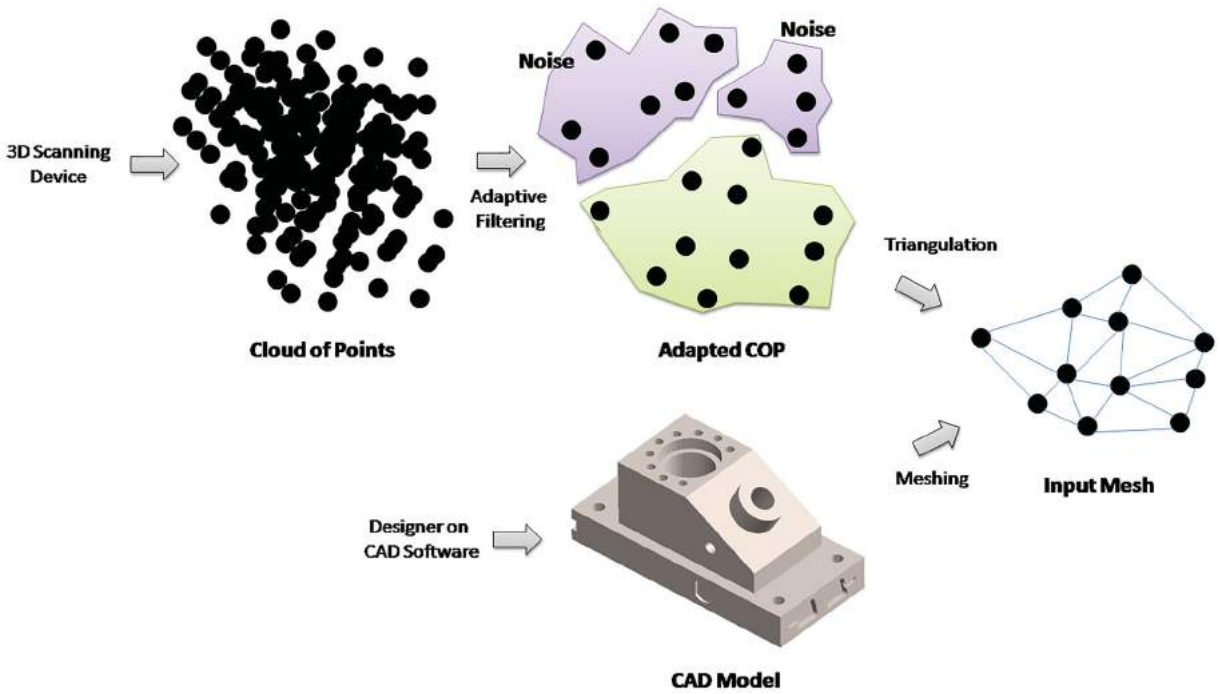


Figure 4. Input preparation: a triangulated linear mesh.

diffusion equation, or namely the heat equation defined on a compact Riemannian 2-manifold (\mathcal{M}, g) embedded in \mathbb{R}^3 :

$$\frac{\delta U}{\delta t} + \kappa \Delta U = 0 \tag{3.1}$$

where κ is a positive constant, namely the thermal conductivity, and $U(x, t)$ is a real-valued function whose value indicates the temperature of a point $x \in \mathcal{M}$ at a given time t . Here, Δ is the intrinsic Laplace-Beltrami operator acting on differentiable functions defined over \mathcal{M} . That is, for a differentiable function f defined on \mathcal{M} , an explicit formula for Δf in local coordinates is defined to be

$$\Delta f = \frac{1}{\sqrt{|g|}} \sum_{i,j} \partial_i (\sqrt{|g|} g^{ij} \partial_j f) \tag{3.2}$$

where $|g|$ is the determinant of the metric tensor g , and g^{ij} is the components of g^{-1} . It is noted that if the manifold \mathcal{M} is a (Riemannian) submanifold of the Euclidean plane \mathbb{R}^2 with its inherent Euclidean metric, the formula reduces to the well-known Laplacian $\Delta f = \partial_{xx}f + \partial_{yy}f$. For more detailed discussion on the differential operators on Riemannian manifolds, readers are directed to e.g. [3]. Figure 5 shows the heat diffusion for a number vertices in a part mesh after application of a unit heat source.

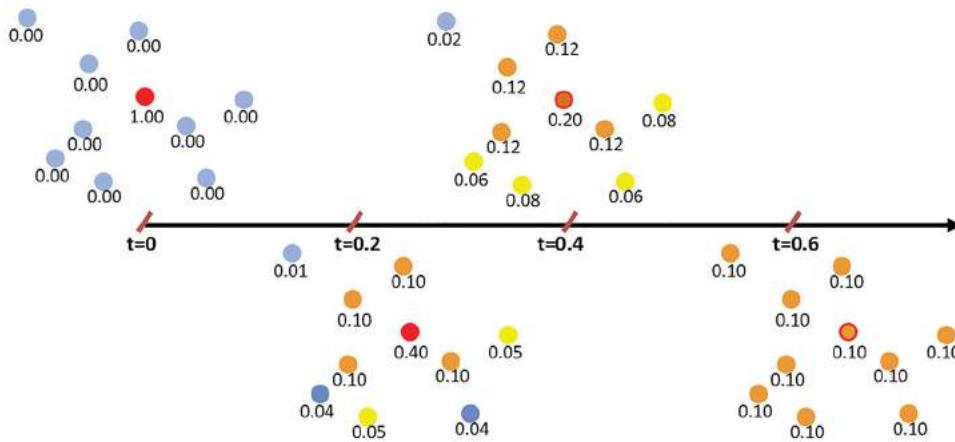


Figure 5. After a unit amount of heat is applied (red dot), heat diffuses and propagates until uniformity is reached.

Figure 6 shows heat diffusion on a part after application of a unit heat at the tip of the sphere applied within Shape Terra at different time intervals.

One of the known solutions for Equation 3.2 is the heat kernel. The heat kernel represents the quantity of heat received by a point after a unit of heat is applied at a certain reference point at time $t = 0$ [9]. It is well known that the solution of Equation 3.1 can be expressed in integral form as:

$$U(x, t) = \int_{\mathcal{M}} H_t(x, y)U(y, 0) dy \quad (3.3)$$

where $H_t(x, y)$ is what so-called heat kernel, whose eigen-decomposition is expressed as

$$H_t(x, y) = \sum_{i=1}^{\infty} e^{-\lambda_i t} \phi_i(x)\phi_i(y) \quad (3.4)$$

where λ_i and ϕ_i are the eigenvalues and the corresponding eigenfunctions of the Laplace-Beltrami operator Δ over \mathcal{M} . Here, it should be noted that $0 \leq \lambda_1 \leq \lambda_2 \leq \dots \leq \infty$ for every kind of manifolds. It should also be noted that for a closed manifold without boundary or for the Neumann boundary conditions the first eigenvalue is always zero, while the first eigenvalue is greater than zero if the Dirichlet boundary conditions exist. Using the heat kernel, we can derive the heat retained by a local area

$D_x \subset \mathcal{M}$ around a point x at a given time instance t . If we assume that the initial heat distribution was a Dirac delta distribution $\delta_x(y)$, i.e. only a source point x has an infinite heat value and the other points have zero heat, and that there is no loss of the net heat, the retained heat value R_x by the local area D_x can be expressed as:

$$R_x(t) = 1 - \int_{\mathcal{M} \setminus D_x} H_t(x, y) dy \quad (3.5)$$

where $\mathcal{M} \setminus D_x$ denotes the set subtraction. This is because the total heat applied at $t = 0$ is:

$$\int_{\mathcal{M}} H_{t=0}(x, y) dy = \int_{\mathcal{M}} \delta_x(y) dy = 1$$

and the net heat is preserved without loss over \mathcal{M} . Therefore, at the end of this stage we would have for each point the amount of heat retained as time elapses, namely $R_x(t)$. A sample heat retention of a point is presented in Figure 7.

3.2. Discretization

The method described above is well formulated with respect to the intrinsic Laplace-Beltrami operator in a continuous domain. Therefore in principle, our method can be applied to any type of discrete domain equipped

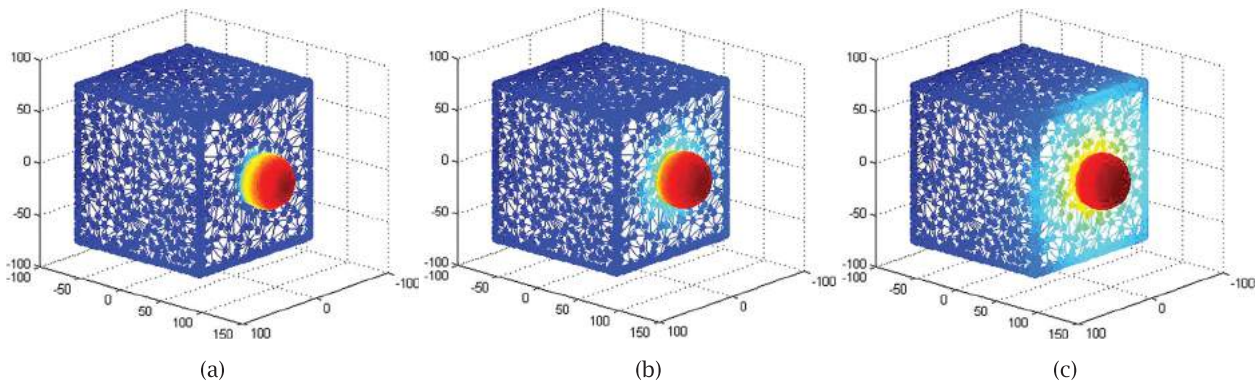


Figure 6. Heat diffusion when a source heat is applied at (a) $t = 0.061$ s, (b) $t = 0.111$ s, (c) $t = 0.201$ s.

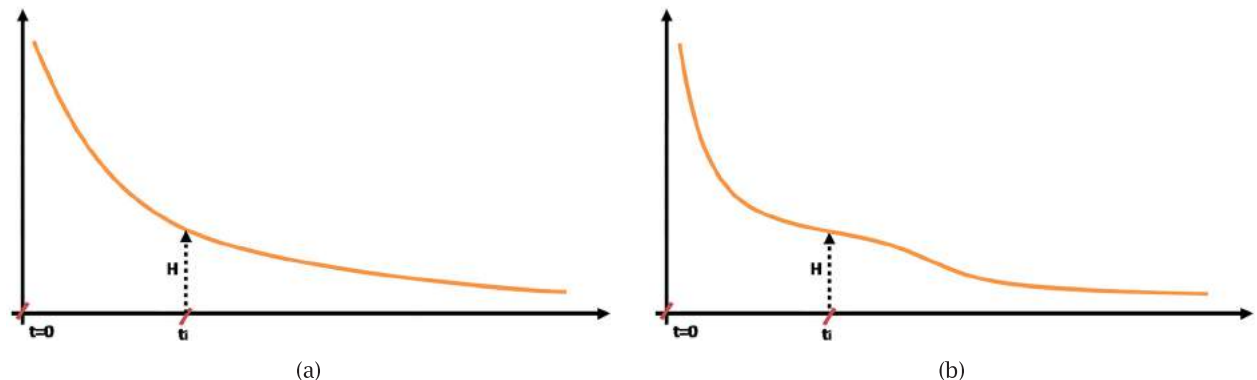


Figure 7. Heat retention at (a) Typical point, (b) Point with resistance areas (typically bottom of a pocket).

with a properly discretized Laplace-Beltrami operator. For more details on the discretization of Laplace-Beltrami operator in domains other than simplicial meshes, readers are directed e.g. to [18] (for point clouds) or to [1] (for polygonal meshes).

The basic assumption for the discretization on a triangular mesh is that the function values are integrated over the local area around each vertex, and assigned to the corresponding vertex. It perfectly migrates fundamental theorems of manifold calculus from the continuous world to discrete domains. In addition, by the term “local area”, we mean the Voronoi cell around a vertex. Upon this basic assumption, we now discretize the Laplace-Beltrami operator Δ . From among the possible discretizations of the Laplace-Beltrami operator, we use a modified Laplacian in the application of the heat kernel. While normally matrices include an indicator to the manifold curvature (the cotangent), we add a mesh uniformity factor to overcome mesh proportionality and skewness. This weight applied to the traditional cotangent value is exhibited by the Voronoi area. Equation 3.6 presents our modification of the Laplacian. Figure 8 presents the geometric elements needed for this equation.

$$L_{ij} = \frac{1}{S_i} \left(\frac{\cot \alpha_{ij} + \cot \beta_{ij}}{2} \right) \quad (3.6)$$

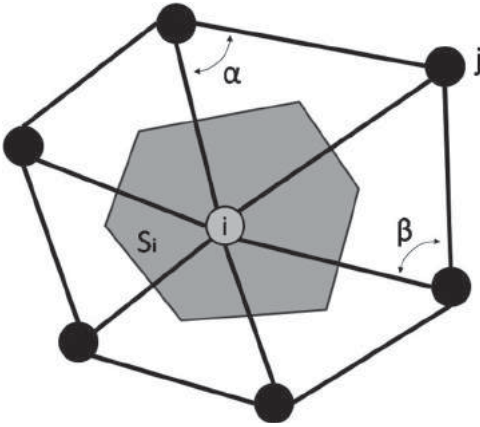


Figure 8. Geometric elements to compute the modified normalized Laplacian.

In the meantime, the heat kernel can be successfully approximated by only a few of the eigenfunctions using the fact that for the first several eigenfunctions would have dominant weight values $e^{-\lambda_i t}$. From the previous works regarding the heat kernel (such as [20]), it is known that it is reasonable to use more than 300 eigenfunctions for the decomposition. Therefore, for all examples and results displayed hereafter, we choose to use only 300 eigenfunctions. This is a trade-off between accuracy and

computational efficiency. Based on the desired performance, the number of eigenfunctions used in Shape Terra can be adjusted accordingly.

On the other hand, Shape Terra gives the ability to specify the time frame and the desired computation steps. Standard values are from $t = 0.001$ to $t = 1$, using a time step $\tau = 0.001$. At each instance t , heat retained at the source R_x is computed and saved in a HKS record matrix. Each point of the starting block is treated separately and used to complete the HKS record. This is the most computationally expensive step. Future efforts will include further optimization steps to enhance computation times of Shape Terra.

3.3. Stage 2: computing the local heat retention level and value

This second stage will measure the persistence P of a point to retain heat and its resistance to losing its heat. Heat retention is defined as an interval where the heat value on a node persists above a minimum threshold. It can be calculated by level or by value. By doing so, we apply persistent homology to extract significant subsets of the global mesh at different time intervals.

3.3.1. Retention level

Retention levels are measured by instances of time where heat at a certain point is still higher than a preset value μ . At the start, heat with a starting value λ is rapidly lost. Next, the heat will persist through a certain time frame (shown in red on Figure 9(a)). Retention levels are computed using Equation 3.7:

$$R_l = \frac{t_i}{\tau} \quad (3.7)$$

Here t_i is the time when heat drops below threshold μ and τ is the Shape Terra computation step.

3.3.2. Retention value

Retention values are measured by the incremental value of heat, until the time where heat drops lower than a preset value μ . It can be computed as the integral of the heat function or the area below the heat curve (shown in red on Figure 9(b)):

$$R_v(x) = \int_0^{t_i} R_x(t) dt$$

3.4. Stage 3: persistence clustering

The third stage will cluster points of similar persistence. The cloud of points is divided into subsets that group adjacent nodes having similar heat values. Adjacency is

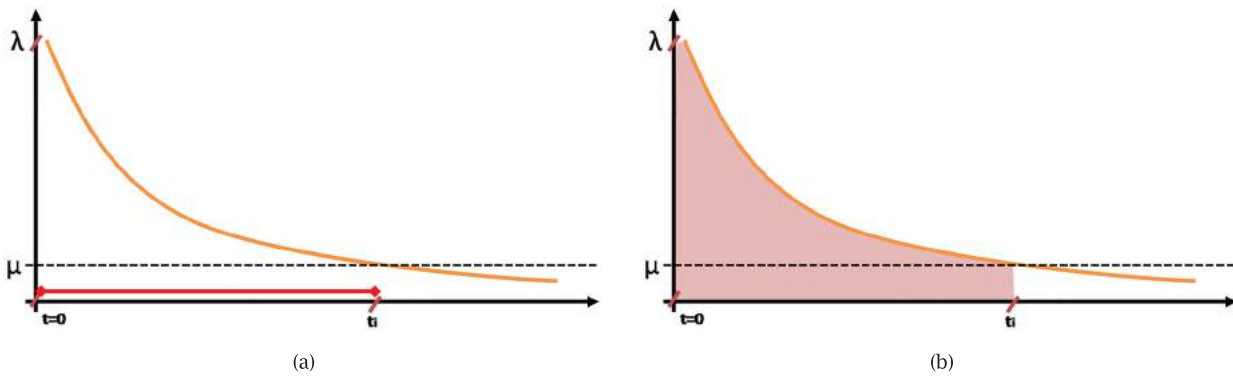


Figure 9. (a) Retention level shown in red. (b) Retention value (area) shown in red.

determined from a connectivity matrix, which is a square matrix containing all nodes with a 1 when nodes are connected and 0 otherwise. Similarity in persistence applies when 2 nodes exhibit a heat value within a defined similarity percentage.

The clustering step is to predict a mass pattern and to prepare the potential shape output. Typically elongated features will have “rings” of points with similar heat values. To demonstrate, we illustrate the principle in Figure 10. The algorithm initiates clustering from the point retaining the most to dissipate heat. All points connected with heat value higher than the matching limit, would be clustered together. When low similarity percentage is computed, features would be completely detected with surrounding elements and noise components. The result shown in step (a) would not be representative of any real feature. As the similarity

percentage is increased, elongated rings in (b) (c) and (d) becomes more distinctive. It is worthwhile to note that the tip of the feature might converge into one heated cluster or get further separated depending on the feature profile. This will be further detailed in stage 4.

Figure 11 shows an example of applying this persistence clustering stage. Figure 11(a) represents the neutral cloud of point of our test part. Figure 11(b) represents the clustering when a 70% similarity factor is applied. We can clearly note that the “tip” of features is identified. The overall most resistant areas constitute the tips of the parts. Figure 11(c) shows the split of clusters into more refined rings. Symmetrical tips and cross sections are noted to have uniform rings. Figure 11(d) shows a further split of the clusters and a more refined clustering. This would enable a more accurate clustering of validated clusters.

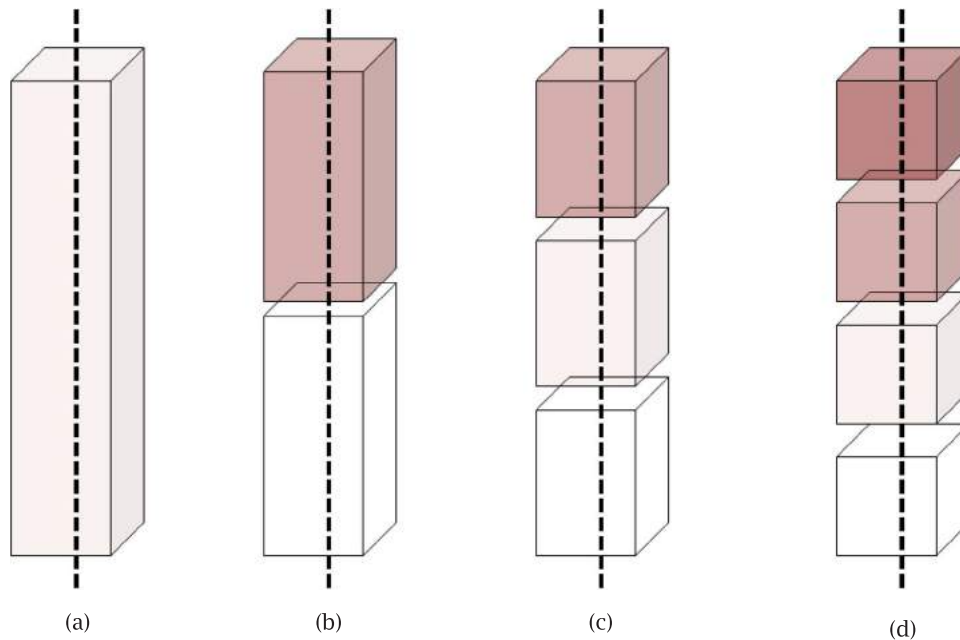


Figure 10. As persistence similarity increases, clustering is refined (a) Low similarity, (b) Medium similarity, (c) Medium-high similarity, (d) High similarity.

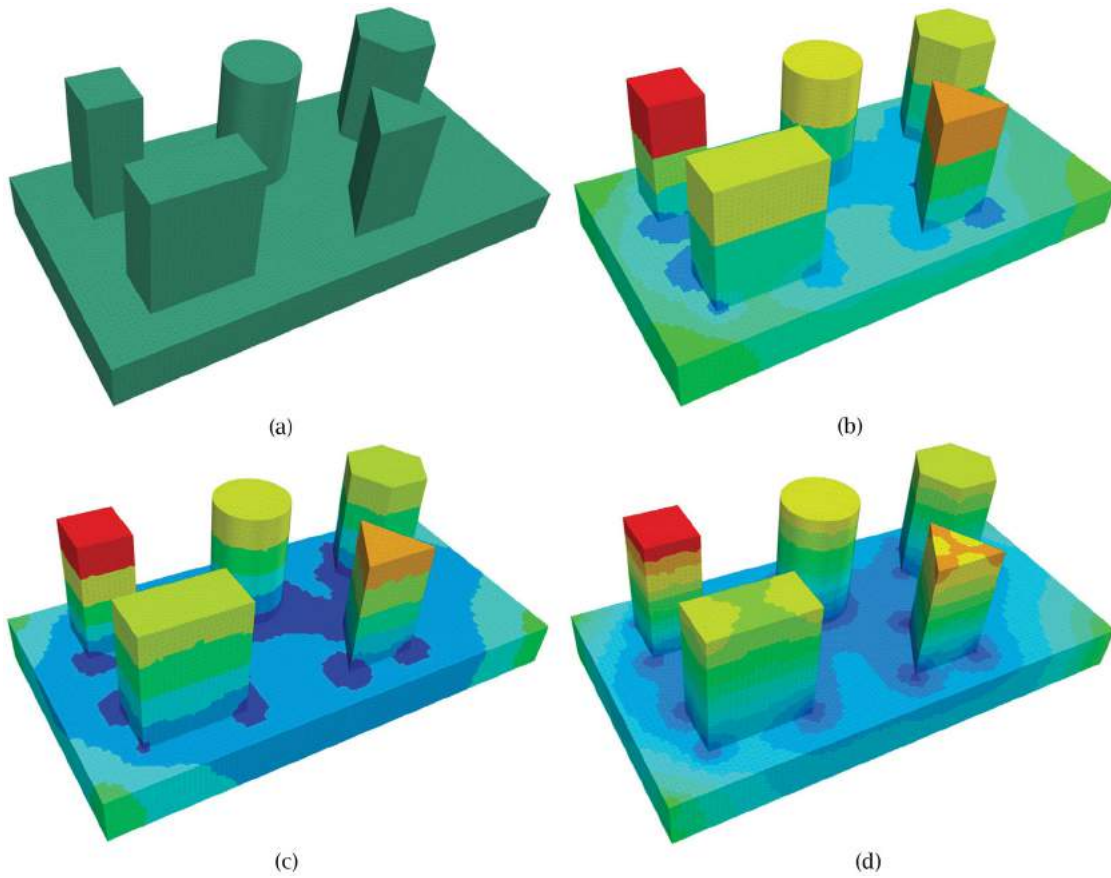


Figure 11. Sample persistence clustering. (a) Neutral, (b) 70% Similarity, (c) 80% Similarity, (d) 90% Similarity.

3.5. Stage 4: multiscale filtering

This stage is the most important in the recognition step. We survey potential features through a multiscale filtering technique. The latter is used to separate clusters that form the features from other clusters. We use a methodology of separating cold from warm bodies based on network graphs. The concept is to recognize and split

feature islands. The latter is defined as the potential feature including the starting heated zone (Red tip zone in Figure 10(d)).

The multiscale filtering first identifies the coldest weighted body. Figure 13 illustrates the concept on the part of Figure 12. The concept is to find split islands by discarding interconnected subsets with more than two

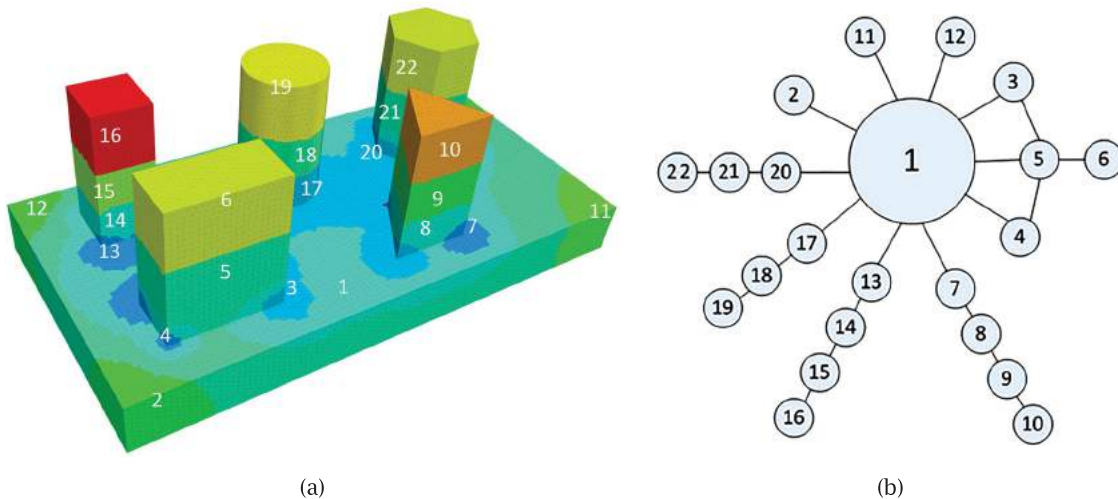


Figure 12. (a) Identifying clusters and evaluating their average heat persistence, (b) Network graph for clusters at selected similarity.

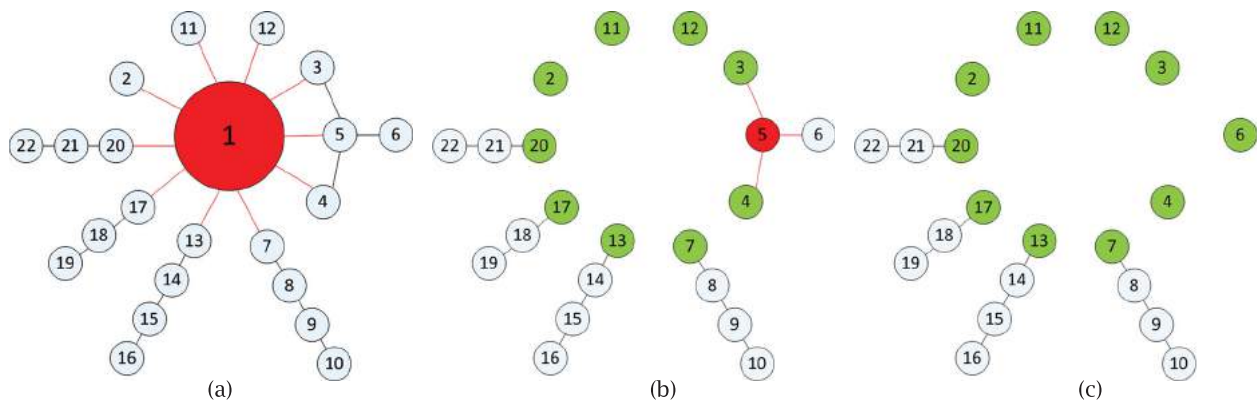


Figure 13. Splitting scheme for interconnected clusters.

unidirectional flows. The scheme shows that first the coldest weighted body is identified, and next, it is discarded and all its connections are canceled. The new starting points are identified as the previous connections. Remaining new starting points are disabled (green) if they do not hold more than one directional flow. The algorithm continues until the last instance is validated. The output may include some meaningless clusters identified at a typically low similarity level, see Figure 14.

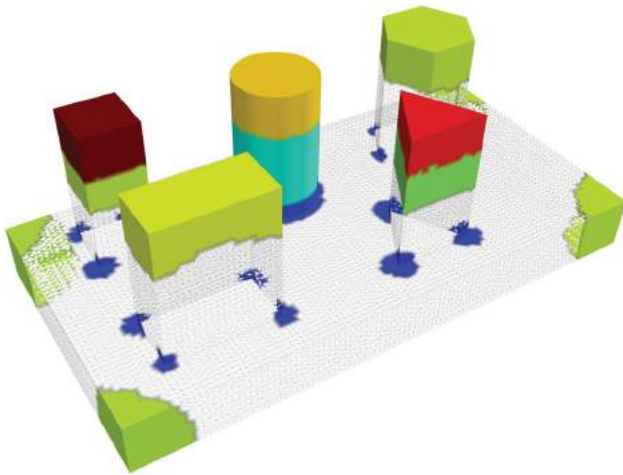


Figure 14. Multiscale filtering sample result at 70% similarity.

At this stage, the algorithm issues a merge request: It propagates the pre identified tips and runs similarity and inclusivity tests for similar subsets at incremented persistence similarity subsets. The algorithm dynamically searches for the optimal clusters enclosing most pre identified sets. Figure 15 shows the multiscale filtering set results for the sample part.

3.6. Stage 5: feature recognition

The direction of a feature is determined by obtaining the line that best fits the points present in the cluster of

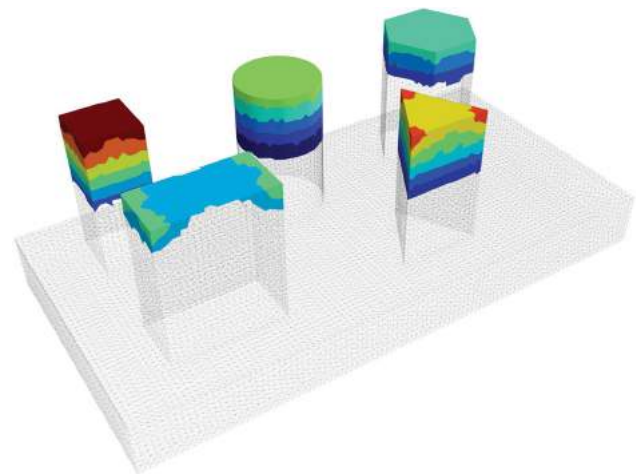


Figure 15. Final result of stage 4 following the application of the multiscale filtering.

clusters. The Singular Value Decomposition method was used to fit the points. The cross-section of a feature is determined by projecting the nodes of the cluster on a plane normal to the direction vector. After obtaining the clusters, the center of gravity of each cluster is computed. The results for a sample part are shown in Figure 16. It was noticed that a similarity of 85% retains all necessary clusters after filtering. A lower percentage leads to missing clusters and a higher percentage leads to surplus clusters.

4. Current results

Five features represent 95% of mechanical features found in mechanical products: Protrusions, Pockets, Dimples, Chamfers/Fillets and Ribs. A database of parts (a selection is shown in Figure 17) exhibiting those features was created for Shape Terra testing purposes. More complex features will be left for future works.

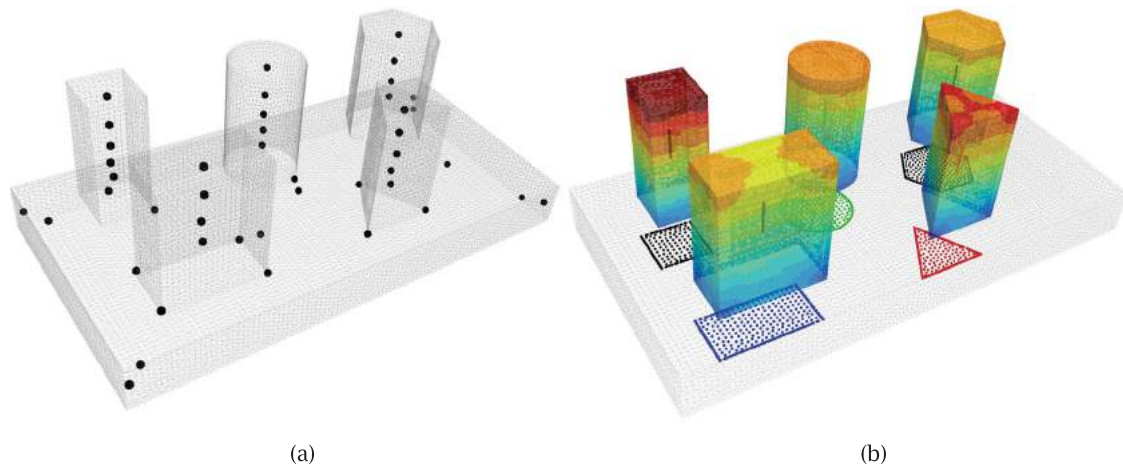


Figure 16. (a) Cluster centers of gravity, (b) Recognized features and attributes.

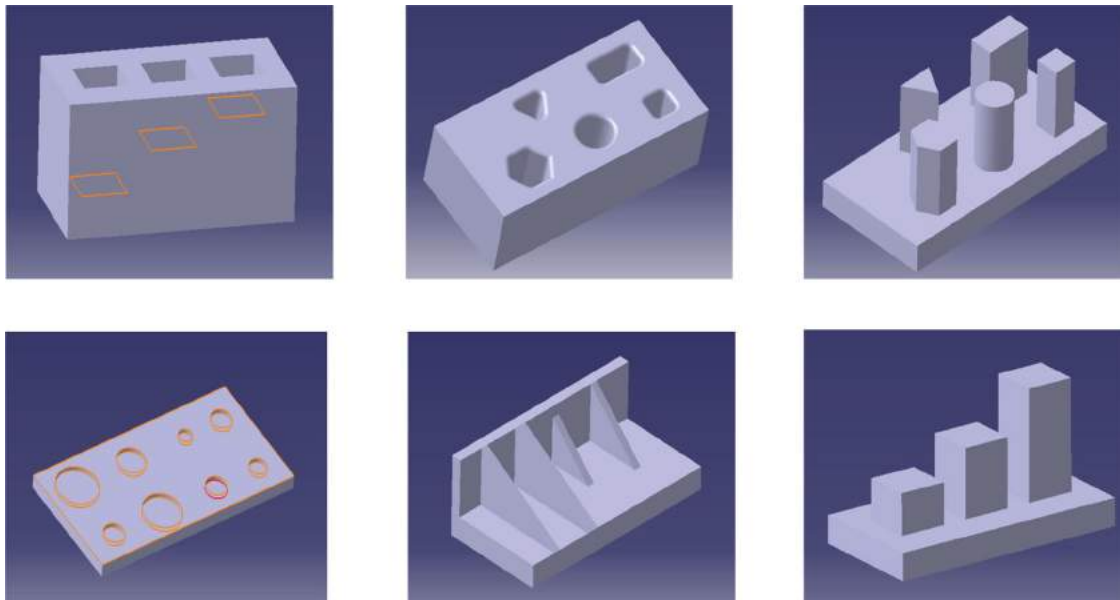


Figure 17. Selection of Shape Terra CAD database.

The software was developed in Python to facilitate the creation of an online WebCAD tool. The software is completely standalone and not connected to any current CAD software. The current effort is at the demonstration a testing stage; further refinements are needed to handle complexity of future parts. Table 1 shows the results and recognition on different selected test parts.

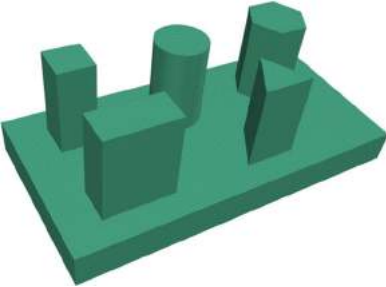
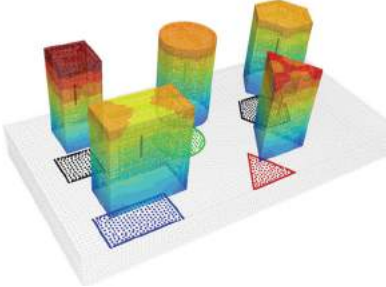
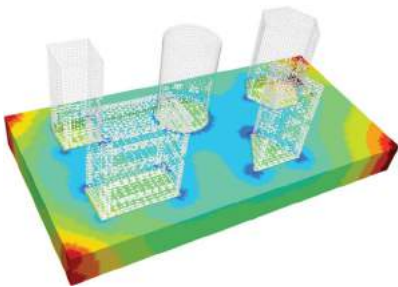
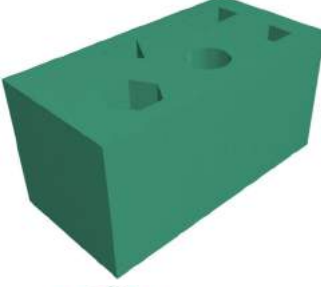
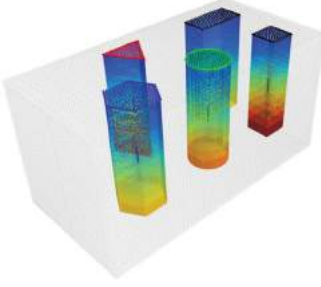
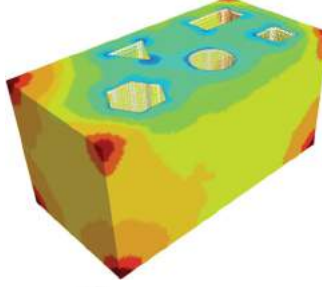
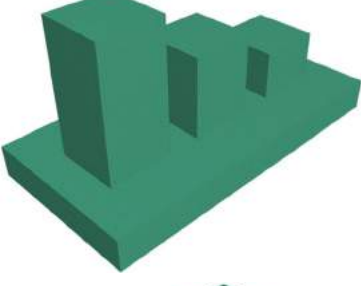
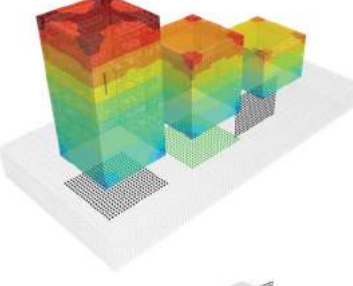
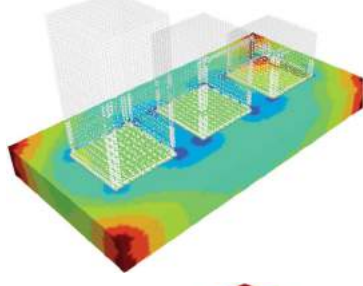
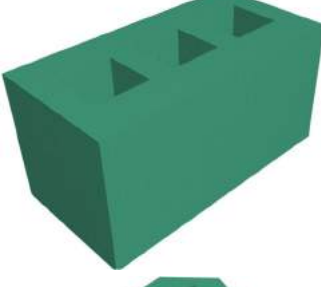
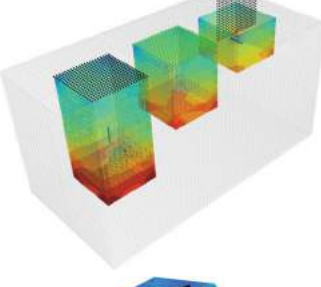
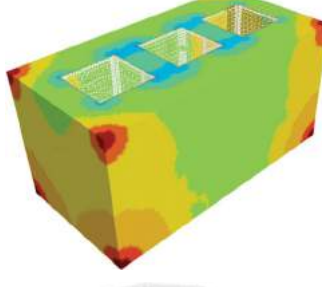
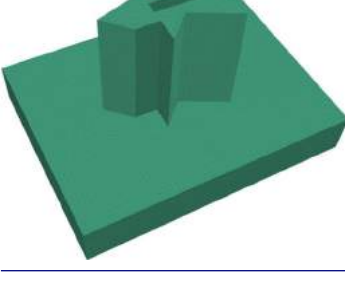
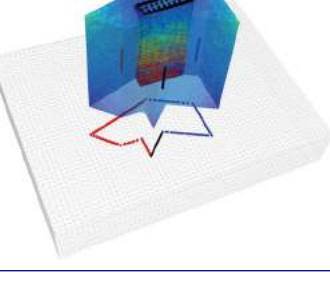
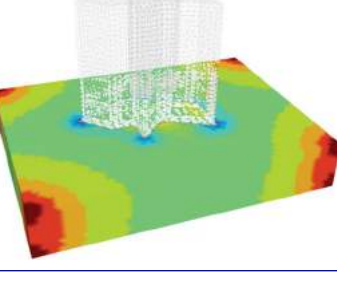
5. Conclusion

This article presented a novel technique to recognize mechanical features. First, a literature review on the state of the art of feature recognition was presented. It highlighted the recent applications within multimedia shape benchmarking, as well as traditional shape signature and descriptors methods. We then differentiated

between the two domains and highlighted the major dissimilarities. The literature review also discussed a potential coupling with engineering analysis techniques. The latter included, but was not limited to, the usage of amalgams in optimizing the model order reduction methodology. The selected analysis approach was then presented in detail. The technique includes five stages: Heat Kernel Signature, persistence definition and computation, persistence clustering and resulting subsets, multiscale filtering, feature recognition, and determination of attributes. Shape Terra results were discussed based on analysis of mechanical parts from a CAD database.

The effort presented in this paper is still considered in its early stages. It sheds light and presents a first step approach to recognize and identify shapes of mechanical

Table 1. Selected results on preset parts.

Mesh	Recognized Features	Leftover for further processing
		
		
		
		
		

importance. In future work, we will focus on several enhancement elements, such as:

- Embedding amalgams to facilitate model order reduction and selection of optimal eigenvalues and eigenvectors
- Adding a post processing stage to correct inaccurate leftovers. Once a feature is computed and set, reconstructing it geometrically and performing corrective subset attribution will refine leftover errors and further reduce unidentified subsets

- Introducing special feature recognition capabilities and connecting it to trade databases. An example would be elementary thin features or rib features that are abundant in aerospace industry

Acknowledgements

The authors would like to acknowledge the support of Barend-Jan van Bruchem, Joe Khalife, and Reef Khairallah.

ORCID

Ramy Harik  <http://orcid.org/0000-0003-1452-9653>

Yang Shi  <http://orcid.org/0000-0002-9579-9403>

Stephen Baek  <http://orcid.org/0000-0002-4758-4539>

References

- [1] Alexa, M.; Wardetzky, M.: Discrete laplacians on general polygonal meshes, *ACM Transactions on Graphics*, 30(4), 2011, 102:1–102:10. <http://dx.doi.org/10.1145/2010324.1964997>
- [2] Belkin, M.; Sun, J.; Wang, Y.: Discrete laplace operator on meshed surfaces, *Proceedings of the Twenty-fourth Annual Symposium on Computational Geometry, SCG '08*, 2008, 278–287. <http://dx.doi.org/10.1145/1377676.1377725>
- [3] Boothby, W. M.: *An introduction to differentiable manifolds and Riemannian geometry*, Academic Press, Orlando, Florida, 1986.
- [4] Boyer, E.; Bronstein, A. M.; Bronstein, M. M.; Bustos, B.; Darom, T.; Horaud, R.; Hotz, I.; Keller, Y.; Keustermans, J.; Kovnatsky, A.; Litmany, R.; Reininghaus, J.; Sipiran, I.; Smeets, D.; Suetens, P.; Vandermeulen, D.; Zaharescu, A.; Zobel, V.: SHREC '11: Robust Feature Detection and Description Benchmark, *Eurographics Workshop on 3D Object Retrieval*, 2011, 71–78. <http://dx.doi.org/10.2312/3DOR/3DOR11/071-078>
- [5] Bronstein, M.; Kokkinos, I.: Scale-invariant heat kernel signatures for non-rigid shape recognition, *Computer Vision and Pattern Recognition (CVPR)*, 2010 IEEE Conference on, 2010, 1704–1711. <http://dx.doi.org/10.1109/CVPR.2010.5539838>
- [6] Cagliari, F.; Di Fabio, B.; Ferri, M.: One-dimensional reduction of multidimensional persistent homology, *Proceedings of the American Mathematical Society*, 138(8), 2010, 3003–3017. <http://dx.doi.org/10.1090/S0002-9939-10-10312-8>
- [7] Carlsson, G.; de Silva, V.; Morozov, D.: Zigzag persistent homology and real-valued functions, *Proceedings of the Twenty-fifth Annual Symposium on Computational Geometry, SCG '09*, 2009, 247–256. <http://dx.doi.org/10.1145/1542362.1542408>
- [8] Chen, C.; Freedman, D.: Measuring and computing natural generators for homology groups, *Computational Geometry*, 43(2), 2010, 169–181. <http://dx.doi.org/10.1016/j.comgeo.2009.06.004>
- [9] Dey, T. K.; Li, K.; Luo, C.; Ranjan, P.; Safa, I.; Wang, Y.: Persistent heat signature for pose-oblivious matching of incomplete models, *Computer Graphics Forum*, 29(5), 2010, 1545–1554. <http://dx.doi.org/10.1111/j.1467-8659.2010.01763.x>
- [10] Edelsbrunner, H.; Letscher, D.; Zomorodian, A.: Topological persistence and simplification, *Discrete & Computational Geometry*, 28(4), 2002, 511–533. <http://dx.doi.org/10.1007/s00454-002-2885-2>
- [11] Fang, Y.; Sun, M.; Ramani, K.: Temperature distribution descriptor for robust 3D shape retrieval, *Computer Vision and Pattern Recognition Workshops (CVPRW)*, 2011 IEEE Computer Society Conference on, 2011, 9–16. <http://dx.doi.org/10.1109/CVPRW.2011.5981684>
- [12] Gal, R.; Shamir, A.; Cohen-Or, D.: Pose-oblivious shape signature, *Visualization and Computer Graphics, IEEE Transactions on*, 13(2), 2007, 261–271. <http://dx.doi.org/10.1109/TVCG.2007.45>
- [13] Harik, R. F.: Specified functions for an automated process planning generation system: Application on aircraft structural parts, software prototype within the RNTL Usiquick project, Ph.D. thesis, University Henri Poincare, Nancy, France, 2007. <https://tel.archives-ouvertes.fr/tel-00173161/document>
- [14] Harik, R. F.; Derigent, W. J. E.; Ris, G.: Computer aided process planning in aircraft manufacturing, *Computer-Aided Design and Applications*, 5(6), 2008, 953–962. <http://dx.doi.org/10.3722/cadaps.2008.953-962>
- [15] Hudson, B.; Miller, G. L.; Oudot, S. Y.; Sheehy, D. R.: Mesh-enhanced persistent homology, 2009. <http://donsheehy.net/research/hudson09mesh-fwcg.pdf>
- [16] Iyer, N.; Jayanti, S.; Lou, K.; Kalyanaraman, Y.; Ramani, K.: Three-dimensional shape searching: state-of-the-art review and future trends, *Computer-Aided Design*, 37(5), 2005, 509–530. <http://dx.doi.org/10.1016/j.cad.2004.07.002>
- [17] Jain, V.; Zhang, H.: A spectral approach to shape-based retrieval of articulated 3D models, *Computer-Aided Design*, 39(5), 2007, 398–407. <http://dx.doi.org/10.1016/j.cad.2007.02.009>
- [18] Liu, K.; Boehm, J.: A new framework for interactive segmentation of point clouds, *ISPRS- International Archives of the Photogrammetry, Remote Sensing and Spatial Information Sciences*, 1, 2014, 357–362. <http://dx.doi.org/10.5194/isprsarchives-XL-5-357-2014>
- [19] Rustamov, R. M.: Laplace-beltrami eigenfunctions for deformation invariant shape representation, *Proceedings of the fifth Eurographics symposium on Geometry processing*, 2007, 225–233. <http://dl.acm.org/citation.cfm?id=1281991.1282022>
- [20] Sun, J.; Ovsjanikov, M.; and Guibas, L.: A Concise and Provably Informative Multi-Scale Signature Based on Heat Diffusion, *Computer Graphics Forum*, 28(5), 2009, 1383–1392. <http://dx.doi.org/10.1111/j.1467-8659.2009.01515.x>
- [21] Young, A.: Eigenvalues and the heat kernel, 2003. https://www.researchgate.net/publication/265141656_Eigenvalues_and_the_Heat_Kernel
- [22] Zomorodian, A.: Fast construction of the vietoris-rips complex, *Computers & Graphics*, 34(3), 2010, 263–271. <http://dx.doi.org/10.1016/j.cag.2010.03.007>
- [23] Zomorodian, A.; Carlsson, G.: Computing persistent homology, *Discrete & Computational Geometry*, 33(2), 2005, 249–274. <http://dx.doi.org/10.1007/s00454-004-1146-y>